2021-12

Freak waves caused by reflection

Andrade, David

10.1016/j.coastaleng.2021.104004
Coastal Engineering
Elsevier BV

Highlights

Freak waves caused by reflection

David Andrade,Raphael Stuhlmeier,Michael Stiassnie

- Reflection can serve as a mechanism for generating inhomogeneity and thereby as a generator of freak waves.
- There are two regimes where the effective behavior of the averaged wave field is linear: in shallow depths or when the attacking spectrum is broad.
- In deep water and when the attacking spectrum is narrow, the inhomogeneous statistics are nonlinear, thereby increasing the probability of freak wave occurrence.

Freak waves caused by reflection*

David Andrade[a,*], Raphael Stuhlmeier[b] and Michael Stiassnie[a]

[a]Department of Civil and Environmental Engineering, Technion, Haifa, Israel
[b]Centre for Mathematical Sciences, University of Plymouth, Plymouth PL4 8AA, UK

ARTICLE INFO

Keywords:
Reflection of waves
CSY equation
Freak waves

ABSTRACT

We study the temporal distribution of wave energy in a wave field that is generated by the reflection of a wave spectrum from a vertical wall. Weakly nonlinear wave fields over finite, constant depth are considered, and the reflection induces large correlations between different wave components of the wave field. The nonlinear time evolution of such an inhomogeneous random wave field is studied by means of an equation developed by Crawford, Saffman and Yuen in 1980. We show that, depending on the spectrum and the water depth, there is a significant increase in the probability of freak waves, whose height is more than twice the significant wave height, created by the reflection off the wall.

1. Introduction

Coastal regions around the world are densely settled, popular for leisure activities, and home to critical infrastructure. While these locations thrive because of their proximity to the sea, that sea also presents a threat which must be guarded against. Coastal defenses in the form of sea walls and breakwaters are erected to protect against incursions of the sea, and yet the risk of damage looks set to increase as sea levels rise (Dawson et al., 2016). Damage to the seawall at Dawlish during winter storms in 2014 led to closures of the London to Penzance railway, the sole rail link between Devon and Cornwall and the rest of England, for two months, and caused significant socio-economic damage to the South West. Such coastal defenses protect more than 1000 km of the British coast, and many other coastlines worldwide.

The need to study the effects of waves on sea walls is clear. While modern computational fluid dynamics simulations can shed light on details of a wave impact (Liu et al., 2019), and numerous experimental studies have been performed on the forces exerted by breaking waves on vertical walls (Hattori et al., 1994; Bullock et al., 2007), the longevity of defensive structures in severe storms must also be considered from a statistical perspective.

In this article we will investigate the probability distribution of wave heights caused by reflection, with a view to informing inhabitants of coastal regions of hazardous ocean conditions. The model under investigation has as input a wave spectrum for the attacking waves and a constant water depth. The output is the time evolution of a correlation matrix, from which the spectral evolution can be extracted, including a time series of the variance of the free surface elevation and the probability of exceedance for the wave height. The reflection is modelled through a Neumann boundary condition at the solid, vertical wall. Different types of reflection are possible but we do not investigate them here.

The equation behind this model was originally derived by *Crawford*, *Saffman*, and *Yuen* (1980), and we therefore call it the CSY equation. It models the nonlinear evolution of a statistically inhomogeneous random wave field, i.e. a random wave field including non-trivial correlations between different wave components.

To the best of our knowledge, only two equations have been developed to model inhomogenous ocean wave fields: the CSY equation and the Alber equation, see Alber (1978). In both of these models, when the underlying sea state is statistically homogeneous, all the wave components are completely independent of each other and the wave heights follow a Rayleigh distribution to lowest order. These model equations can only produce a different outcome when correlations between wave modes are introduced into the system, the effects of which have gained increasing attention in recent years (see e.g. Ribal et al. (2013); Gramstad (2017); Athanassoulis and Gramstad (2021)). The source of such

*Funding: This work was supported by the Israeli Science Foundation Grant 261/17; and EPSRC Grant EP/V012770/1.
*Corresponding author
deandradep@gmail.com (D. Andrade); raphael.stuhlmeier@plymouth.ac.uk (R. Stuhlmeier); miky@technion.ac.il (M. Stiassnie)
ORCID(s): 0000-0002-9486-8200 (D. Andrade); 0000-0002-6568-1543 (R. Stuhlmeier)

initial correlations is not yet fully understood, despite some preliminary results of Regev et al. (2008) and Andrade and Stiassnie (2020a). Obstacles, such as walls, offer a natural way to correlate different wave components, thus naturally requiring the use of inhomogeneous evolution equations for the study of the resulting wave fields.

This paper is organized as follows: in Section 2, we introduce the linear water wave problem, discuss the influence of a vertical wall, and introduce the free surface variance. Section 3 discusses the weakly nonlinear theory for deterministic (Zakharov equation) and stochastic wave fields (CSY equation). The variance of the free surface, a key concept in the subsequent discussion, is introduced in Section 3.2. The reflection of a wave spectrum modelled via the CSY equation is treated in Section 4, which presents numerical simulations for numerous cases of interest. These numerical simulations give rise to changes in freak-wave statistics, which are the topic of Section 5, which explores the departures from homogeneity and their influence on extreme waves. Finally, Section 6 presents some discussions and concluding remarks. Kernels used in the finite-depth computations are presented in an Appendix.

2. Linear theory

The problem of linear water waves propagating over constant depth h and reflected from a vertical wall at $x = 0$ is governed by the following equations

$$\triangle\phi = 0, \quad \text{in } -\infty < x < 0 \text{ and } -h < z < 0, \tag{1}$$

$$\phi_z = 0, \quad \text{on } z = -h, \tag{2}$$

$$\eta_t = \phi_z, \quad \text{on } z = 0, \tag{3}$$

$$\phi_t = -g\eta, \quad \text{on } z = 0, \tag{4}$$

$$\phi_x = 0, \quad \text{on } x = 0 \text{ and all } t. \tag{5}$$

In these equations $\eta(x,t)$ is the free surface elevation, $\phi(x,z,t)$ is the velocity potential and g is the acceleration due to gravity, for which we will use the numerical value $g = 9.81\ \mathrm{ms}^{-2}$. Note that by differentiating equation (4) with respect to x it follows that $\eta_x(0,t) = 0$.

A solution of these equations, suitable for numerical computation, can be obtained as follows. Given N different waves with positive wave numbers $k_1, \dots, k_N$, the profile of the incoming wave field is given by superposition:

$$\eta_I(x,t) = \frac{1}{2\pi}\sum_{j=1}^{N}\sqrt{\frac{\omega_j}{2g}}B_j e^{ik_j x}e^{-i\omega_j t} + c.c. \tag{6}$$

where $c.c.$ denotes the complex conjugate of the preceding expression. This solves equations (1) - (4) provided that the frequencies ω_j and the wave numbers k_j satisfy the dispersion relation

$$\omega^2 = gk\tanh(kh). \tag{7}$$

In equation (6) the complex amplitude B_j is related to the amplitude a_j and phase χ_j of each wave, by means of the following relations, see Mei et al. (2018) equation (14.7.39):

$$a_j = \frac{1}{\pi}\sqrt{\frac{\omega_j}{2g}}|B_j|. \tag{8}$$

$$\chi_j = \arg(B_j). \tag{9}$$

In order to enforce the boundary condition at $x = 0$ we use the method of images. Since the problem is linear, this amounts to adding a mirror reflection of the incoming waves, thus defining the reflected wave field by

$$\eta_R(x,t) = \eta_I(-x,t) = \frac{1}{2\pi}\sum_{j=1}^{N}\sqrt{\frac{\omega_j}{2g}}B_j e^{-ik_j x}e^{-i\omega_j t} + c.c. \tag{10}$$

The free surface is then given by

$$\eta = \eta_I + \eta_R = \frac{1}{\pi}\sum_{j=1}^{N}\sqrt{\frac{\omega_j}{2g}}B_j\cos(k_j x)e^{-i\omega_j t} + c.c. \tag{11}$$

Note that the free surface is an even function of x and so $\eta_x(0,t) = 0$. It is written as a superposition of simple standing waves defined for all x. Also note that $\eta(0) = 2\eta_I(0)$, so the amplitude of the standing waves is twice the amplitude of the incident waves.

We now turn to the stochastic case, where we let $B_1, \dots, B_N$ be independent, mean zero, random variables and $\langle\cdot\rangle$ denote an ensemble average. We are interested in obtaining the statistics of the free surface at the wall, i.e. at $x = 0$.

The first order moment, i.e. the mean surface elevation, is zero since $\langle B_j\rangle = 0$, for every $j = 1, \dots, N$. The second order moment, i.e. the variance of the free surface is

$$\rho_0(x) = \langle \eta^2(x,t)\rangle = \frac{1}{2g\pi^2}\left[\sum_{j=1}^{N} \omega_j C_j \left(1 + \cos(2k_j x)\right)\right]. \tag{12}$$

This equation is obtained by using the independence of the complex amplitudes, so that $\langle B_i B_j^*\rangle = 0$ for all $i \neq j$, and denoting by $C_j = \langle |B_j|^2\rangle$ the variance of each B_j for $j = 1, \dots, N$. This variance can be related directly to the amplitude of each mode via

$$C_j = \frac{2g\pi^2}{\omega_j}\langle a_j^2\rangle. \tag{13}$$

Note that the variance of the free surface does not depend on t, even though η does. At $x = 0$, the variance is

$$\rho_0(0) = \frac{1}{g\pi^2}\sum_{j=1}^{N} \omega_j C_j. \tag{14}$$

This variance is four times larger than the variance of the purely incident wave field.

3. Nonlinear theory

The method of images provides more than just a technique for addressing boundary conditions. It provides the insight that the problem on the half line, i.e. $x < 0$ can be viewed as a problem on the full line by reflecting the waves along the line $x = 0$. Experimental and numerical work by Christou et al. (2009) has demonstrated the utility of this approach in treating reflection of waves from a vertical wall. This is convenient since, in the nonlinear case, the free surface elevation is given by the following equation

$$\eta(x,t) = \frac{1}{2\pi}\sum_{j=-N}^{N} \sqrt{\frac{\omega_j}{2g}} B_j(t) e^{i(k_j x - \omega_j t)} + c.c. \tag{15}$$

Here and in the following, the index $j = 0$ is excluded from every sum sign. The principal difference with the linear case is that the complex amplitudes are now time dependent. Their evolution is governed by the Zakharov equation, see Zakharov (1968), which reduces in the discretised form to the following system of nonlinear ordinary differential equations

$$\frac{d}{dt}B_j = -i\sum_{m,n,p=-N}^{N} T_{j,m,n,p}\,\delta_{j,m}^{n,p}\, e^{i\Delta_{j,m}^{n,p} t} B_m^* B_n B_p, \quad \text{for } j = -N, \dots, N,\ j \neq 0. \tag{16}$$

Here $\delta_{j,m}^{n,p}$ is the Kronecker delta

$$\delta_{j,m}^{n,p} = \begin{cases} 1 & \text{if } k_j + k_m = k_n + k_p, \\ 0 & \text{otherwise,} \end{cases} \tag{17}$$

which imposes a resonance condition on quartets of waves. The frequency detuning is $\Delta_{j,m}^{n,p} = \omega_j + \omega_m - \omega_n - \omega_p$ and $T_{j,m,n,p}$ is a kernel which encapsulates the water wave problem up to third order in nonlinearity (see Mei et al. (2018), Ch. 14 for a detailed derivation).

In the original Zakharov equation the kernel was derived for infinite depth. In finite depth, the symmetric kernels $T_{j,j,j,j}$ and $T_{j,m,j,m}$ are not uniquely defined, and must be treated separately. This delicate issue was first explored by Janssen and Onorato (2007) and Stiassnie and Gramstad (2009), and further details, including detailed expressions for the kernels, are given in the Appendix. Other values of the kernel for non-symmetric quartets $k_j + k_m = k_n + k_p$ with j, m, n and p distinct are well defined and given in Krasitskii (1994) or Mei et al. (2018).

The kernel $T_{p,p,p,p}$, which governs modulational instability of a narrow-banded wave train, changes sign at $k_p h = 1.363$. For shallower depths $h < 1.363/k_p$ we see the disappearance of nonlinear focusing, as reported in Janssen and Onorato (2007), which represents the diminishing contribution of four wave interactions as depth decreases.

The deterministic Zakharov equation requires the provision of suitable initial conditions, from which the time evolution may be computed. In the presence of a wall these initial conditions must satisfy the following symmetry condition:

$$B_{-j} = B_j, \quad \text{for all } j = 1, \dots, N. \tag{18}$$

It can be shown that this symmetry condition is preserved by the Zakharov equation, i.e., any solution that satisfies relation (18) at $t = 0$, satisfies it for all $t > 0$, ensuring that the Neumann boundary condition at $x = 0$ is always satisfied.

3.1. The CSY equation

The development of a statistical theory for inhomogeneous, nonlinear waves by Crawford et al. (1980), culminated in an equation for the one-time, two-wave number correlation function which we call the CSY equation. Following their derivation of the equation, we assume that the complex amplitudes $B_j(t)$ are mean zero random variables. Since the first order moments vanish, the next quantities of interest are the second order moments, also known as the one-time two-wave number correlation functions

$$R_{ij}(t) = \langle B_i(t) B_j^*(t) \rangle. \tag{19}$$

Note that $R_{ij} = R_{ji}^*$ and we assume that $\langle B_i B_j \rangle = 0$, in accordance with the random phase model[1]. The CSY equation is obtained under the following moment closure hypothesis, which is assumed to be valid throughout the evolution of the system

$$\langle B_j^* B_m^* B_n B_p \rangle = R_{nj} R_{pm} + R_{pj} R_{nm}. \tag{20}$$

Note that the Gaussian distribution satisfies this condition exactly, so this closure is consistent with assuming that the wave field is nearly Gaussian.

The equation that governs the time evolution of the correlation R_{ij}, for all $i, j = -N, \dots, N$ is:

$$\frac{d}{dt} R_{ij} = -2i \sum_{m,n,p=-N}^{N} T_{i,m,n,p}\, \delta_{i,m}^{n,p}\, e^{-i\Delta_{i,m}^{n,p} t}\, R_{nj} R_{pm} + 2i \sum_{m,n,p=-N}^{N} T_{j,m,n,p}\, \delta_{j,m}^{n,p}\, e^{i\Delta_{j,m}^{n,p} t}\, R_{in} R_{mp}, \tag{21}$$

This is the CSY equation, a system of coupled nonlinear ODEs for the time-evolution of the correlations, which can be integrated numerically for suitable initial conditions. As in the deterministic case the wall induces the following symmetry condition on the solution for all times t:

$$\begin{aligned} R_{-i,-j} &= \langle B_{-i} B_{-j}^* \rangle = \langle B_i B_j^* \rangle = R_{ij}, \quad \text{for all } i, j = -N, \dots, N, \\ R_{-i,j} &= \langle B_{-i} B_j^* \rangle = \langle B_i B_j^* \rangle = R_{ij}, \quad \text{for all } i, j = -N, \dots, N, \\ R_{i,-j} &= \langle B_i B_{-j}^* \rangle = \langle B_i B_j^* \rangle = R_{ij}, \quad \text{for all } i, j = -N, \dots, N. \end{aligned} \tag{22}$$

In order to obtain initial conditions we let all complex amplitudes of the attacking waves be independent of each other so

$$R_{ij}(0) = C_j \delta_i^j, \quad \text{for all } i, j = 1, \dots, N. \tag{23}$$

[1] I.e. the wave modes have random, independent phases uniformly distributed over the interval $[0, 2\pi]$.

This is called the *homogeneity* condition and has the following important consequence: if we restrict ourselves to the attacking waves, only positive wave numbers are considered in equation (21), whereupon the correlation matrix given in equation (23) is a trivial solution of the CSY equation. When the wall is introduced into the system by virtue of relation (22), the amplitudes of the reflected waves are determined, but more importantly *inhomogeneous* correlations between different wave amplitudes are introduced into the system so that the correlation matrix becomes

$$R_{ij} = \begin{cases} C_j, & \text{for } i = j \text{ and } j = -N, \dots, N, \\ C_j, & \text{for } i = -j \text{ and } j = -N, \dots, N, \\ 0, & \text{otherwise.} \end{cases} \tag{24}$$

Such a correlation matrix is not a trivial solution of equation (21) because of the presence of inhomogeneous terms $R_{j,-j}$. Therefore without the reflection, the evolution of the attacking waves is trivial at this order (higher order contributions would lead to homogeneous kinetic equations relevant for much longer time-scales, as described in Gramstad and Stiassnie (2013)). Once reflection is introduced one needs to integrate the CSY equation in time, using the correlation matrix (24) as initial condition, in order to study the combined time evolution of the incident and reflected wave fields. These computations are the subject of the following sections.

3.2. Variance of the free surface

One of the most important features of the CSY equation is that it lets us study the evolution of the variance of the free surface elevation. The significance of the variance is that it is proportional to the energy, see Holthuijsen (2010). The variance is

$$\rho(x,t) = \langle \eta^2 \rangle = \frac{1}{8g\pi^2} \sum_{i,j=-N}^{N} \sqrt{\omega_i \omega_j} \left[R_{ij}\, e^{i\left((k_i - k_j)x - (\omega_i - \omega_j)t\right)} + c.c. \right] \tag{25}$$

Note that at $t = 0$, $\rho(x,0) = \rho_0(x)$ is given by equation (12).

The CSY equation has three known invariants: the total wave action A, momentum $\mathbf{M}$ and a third invariant $\tilde{H}$ related to the Hamiltonian:

$$A = \sum_{j=-N}^{N} R_{jj}, \tag{26}$$

$$\mathbf{M} = \sum_{j=-N}^{N} \mathbf{k}_j R_{jj}, \tag{27}$$

$$\tilde{H} = \sum_{j=-N}^{N} \omega_j R_{jj} - \mathrm{Im}\left[\sum_{j,m,n,p=-N}^{N} T_{j,m,n,p} \delta^{n,p}_{j,m} \Delta^{n,p}_{j,m} \int_0^t e^{i\Delta^{n,p}_{j,m} s} R_{nj} R_{pm}\, ds \right]. \tag{28}$$

These invariants are used to monitor the accuracy of our numerical solutions. Note that the value of the second invariant is always zero due to the reflection. The value of the third can be related to the initial variance of the free surface (14) via

$$\tilde{H} = \sum_{j=-N}^{N} \omega_j R_{jj}(0) = 2g\pi^2 \rho_0(0). \tag{29}$$

4. Reflection of a wave spectrum

Having established a non linear theory for the reflection of random water waves, we investigate the reflection of an attacking JONSWAP spectrum given by,

$$S(k) = \frac{\alpha}{2k^3} \exp\left[-\frac{5}{4} \left(\frac{k}{k_p} \right)^{-2} \right] \gamma^{\exp\left[-\left(\sqrt{\frac{k}{k_p}} - 1 \right)^2 / 2\sigma^2 \right]}. \tag{30}$$

Table 1
Parameters of the JONSWAP spectrum for the example cases considered. Parameters α and γ are energy scale and peak-sharpening parameters, respectively. The corresponding spectra have average wave slope ε, root-mean-square wave height H_{rms}, and significant wave height H_s, all for $k_p = 1\ \mathrm{m}^{-1}$. The subscript 0 refers to the field of linear standing waves, and H_{s0}, H_{rms0} values are observed to be twice the H_s, H_{rms} values. $\rho_0(0)$ denotes the linear variance at the wall $x = 0$. Π is the dimensionless 'width parameter' (3.8) of Ribal et al. (2013).

	Attacking waves						Linear standing wave field		
Case	α	γ	ε	Π	$H_s\,(m)$	$H_{rms}\,(m)$	$\rho_0(0)\,(m^2)$	$H_{s0}\,(m)$	$H_{rms0}\,(m)$
A	0.02	3	0.10	1.95	0.28	0.20	0.020	0.564	0.399
B	0.045	3	0.15	1.3	0.42	0.30	0.045	0.847	0.599
C	0.01	10	0.10	1.1	0.28	0.20	0.020	0.568	0.402
D	0.025	10	0.15	0.73	0.45	0.32	0.051	0.899	0.635

This spectrum, which represents the attacking wave field, is taken for positive wave numbers only.

In all cases $k_p = 1\ \mathrm{m}^{-1}$ is the peak of the spectrum. As JONSWAP parameters we use $\sigma = 0.08$, and two values of γ. When $\gamma = 10$ we refer to the spectrum as narrow banded, and when $\gamma = 3$ we refer to a broad banded spectrum. The choice of these values was influenced by the experiments of Voermans et al. (2020).

For a given spectrum, the typical wave steepness is taken to be

$$\varepsilon = k_p \sqrt{2 \int_0^\infty S(k)\, dk}. \tag{31}$$

Moreover, the variance[2] of the free surface elevation, for the attacking waves, is given by

$$\rho = \int_0^\infty S(k)\, dk. \tag{32}$$

The root-mean-square wave height H_{rms} and significant wave height H_s for the spectrum of attacking waves are given by

$$H_{rms} = \sqrt{8\rho}, \tag{33}$$

$$H_s = 4\sqrt{\rho}. \tag{34}$$

The four cases investigated, each corresponding to different JONSWAP spectra, are presented in table 1 together with the calculated values of H_{rms} and H_s.

From equations (30) and (31) we can show that $\alpha = \alpha(\varepsilon, \gamma)$. Then, based on Buckingham's Pi theorem any dependent variable such as $\rho(0,t)$, can be written as $\tilde{\rho}(0, \sqrt{gk_p}t) = f(\varepsilon, \gamma, k_p h, \sqrt{gk_p}t)$. Note that according to Ribal et al. (2013), in deep water the JONSWAP spectrum must be narrow, meaning that their 'dimensionless width' parameter $\Pi = \varepsilon/\alpha\gamma < 1$. The values of Π are given in table 1.

In order to integrate the CSY equation numerically the wave number domain is discretized into $N = 81$ evenly spaced wave numbers over the interval $[0.25, 2.25]$. The size of each bin is $dk = 0.025\ \mathrm{m}^{-1}$. The variance of the amplitude of the wave k_j is obtained by integrating the spectrum over the bin $[k_j, k_j + dk]$, so

$$\frac{\langle a_j^2 \rangle}{2} = \int_{k_j}^{k_j + dk} S(k)\, dk \approx dk S(k_j). \tag{35}$$

From this and equation (13), one obtains the following relation between $S(k_j)$ and C_j

$$C_j = \frac{4g\pi^2}{\omega_j} S(k_j) dk. \tag{36}$$

[2] Under the assumption of statistical homogeneity.

Table 2
Conservation of the total wave action A and the third invariant $\tilde{H}$, for each of the four cases A–D and four water depths considered, demonstrating the accuracy of the numerical solution.

Case	depth	A	relative error	$\tilde{H}$	relative error
A($\varepsilon = 0.1, \gamma = 3$)	1	0.69	2.69×10^{-13}	1.93	1.20×10^{-9}
	1.8	0.62	2.77×10^{-14}	1.93	8.26×10^{-10}
	3.6	0.60	9.28×10^{-16}	1.93	6.67×10^{-10}
	10	0.60	4.65×10^{-15}	1.93	7.78×10^{-10}
B($\varepsilon = 0.15, \gamma = 3$)	1	1.55	6.05×10^{-13}	4.34	4.72×10^{-9}
	1.8	1.39	6.23×10^{-14}	4.34	4.62×10^{-9}
	3.6	1.34	9.90×10^{-16}	4.34	1.59×10^{-7}
	10	1.34	2.42×10^{-14}	4.34	7.05×10^{-7}
C($\varepsilon = 0.1, \gamma = 10$)	1	0.71	3.86×10^{-13}	1.95	1.49×10^{-9}
	1.8	0.63	8.74×10^{-16}	1.95	6.83×10^{-10}
	3.6	0.62	1.08×10^{-15}	1.95	5.61×10^{-8}
	10	0.63	8.66×10^{-15}	1.95	3.90×10^{-7}
D($\varepsilon = 0.15, \gamma = 10$)	1	1.77	9.59×10^{-13}	4.89	7.08×10^{-9}
	1.8	1.59	5.59×10^{-16}	4.89	8.28×10^{-9}
	3.6	1.54	1.48×10^{-13}	4.89	1.64×10^{-5}
	10	1.54	1.03×10^{-13}	4.89	1.58×10^{-5}

The reflected spectrum is

$$C_{-j} = C_j, \quad \text{for } j = 1, \dots, N, \tag{37}$$

and the initial condition for the numerical solver is now available through equation (24).

The numerical integration of the CSY equation is computed using MATLAB's ode45 routine with relative and absolute tolerances set to 10^{-12}. Although the symmetry condition (22) reduces the number of equations considerably, with $N = 81$ modes for the incoming waves the total number of equations is 1681, each with hundreds of thousands of terms. A modest number of modes is therefore necessary to keep the problem computationally tractable.

No analytical solutions with such a large number of modes are available for the CSY, therefore the accuracy of the numerical scheme is paramount. This accuracy can be quantified by tracking the relative errors of the invariants A and $\tilde{H}$, as given in table 2. The very small errors in A and $\tilde{H}$ observed throughout our simulations – and the fact that the second invariant is zero and is perfectly conserved by the numerical solver – gives confidence in the accuracy of the solution.

The results of the time evolution of the spectrum and the variance of the free surface are plotted in figures 1a, 1b, 2a and 2b. The time domain is $[0, t_f = 1200\,\text{s}]$, which corresponds to between 520 and 600 periods of the peak wave. The panels on the left show plots of the time evolution of the spectrum; the initial spectrum (blue broken line), the spectrum at $t_f = 1200\,\text{s}$ (yellow dotted line) and the red solid line is the time-averaged spectrum

$$\tilde{R}_{jj} = \frac{1}{t_f} \int_0^{t_f} R_{jj}(\tau)\, d\tau. \tag{38}$$

The panels on the right show the time series of the variance at the wall (at $x = 0$) normalized as

$$\tilde{\rho}(0, t) = \rho(0, t)/\rho_0(0), \tag{39}$$

where ρ is given by equation (25) and $\rho_0(0)$ by equation (14). The values of $\rho_0(0)$ are given in table 1.

Note that the spectrum of standing waves is an even function of k. Consequently, figures 1a, 1b, 2a and 2b depict only positive wave numbers (left panels). On the other hand, the plots of the variance are for the field of standing waves, normalized by their linear variance $\rho_0(0)$ (right panels).

For case A with moderately steep waves ($\varepsilon = 0.1$) and a broad spectrum ($\gamma = 3$) the results of the spectral evolution are depicted in figure 1a. These reveal that hardly any interaction takes place, and there is little change in the spectral shape regardless of the depth. The variance shows some rapid oscillations, particularly for greater depth, but there is little overall change.

Increasing the steepness of the attacking waves to $\varepsilon = 0.15$ (case B), has a destabilizing effect which depends on the water depth. From figure 1b one can see that no meaningful interaction occurs for shallower depths of $h = 1$ m and $h = 1.8$ m, due to the absence of strong four-wave interactions. When the depth increases, the change in the spectrum and, more notably, the evolution of the variance, show that some meaningful nonlinear interaction takes place. Considering the variance for depths of $h = 3.6$ m and $h = 10$ m one observes a long warm up period, of about 300 peak periods for $h = 3.6$ m and 200 peak periods for $h = 10$ m. This period is characterized by a steady increase in the maximum oscillations of the variance, as if the oscillations were modulated by a slowly increasing monotonic envelope. Solutions of the CSY equation typically exhibit a warm up period, which has previously been observed in the evolution of degenerate quartets by Stuhlmeier and Stiassnie (2019) and in systems involving many modes studied by Andrade and Stiassnie (2020b) and Andrade and Stiassnie (2020a). It is also reminiscent of the time-evolution of resonant amplitudes for standing waves reported in Bryant and Stiassnie (1994).

Case C considers a narrow spectrum ($\gamma = 10$) of moderately steep waves ($\varepsilon = 0.1$), and the results shown in Figure 2a are similar to those of case B for depths $h = 1$ m, and 1.8 m. For depths of $h = 3.6$ m the warm up period seems to be very long, as the range of the oscillations grows steadily up to the end of the numerical simulation. For $h = 10$ m growth persists until $t = 700$ s, from which point the variance shows a complex oscillatory pattern. On the other hand, the time averaged spectrum is slightly broader, indicating that on average there is energy exchange and a net energy transfer away from the spectral peak.

Once again an increase in the steepness, from $\varepsilon = 0.1$ to $\varepsilon = 0.15$ (case D), as depicted in Figure 2b, has a strong effect on the subsequent nonlinear evolution. For $h = 1$ m the interaction is nearly negligible, while some minor interactions are visible for $h = 1.8$ m. On the other hand, the interaction for depths $h = 3.6$ m and $h = 10$ m is significant. Note that in both cases the warm up period is about 200 s (or about 100 peak periods) and it is followed by rapid, disordered oscillations of the variance capable of reaching up to four times the values of the linear variance. The spectral evolution shows a significant broadening of the spectrum, a clear indication of energy exchange among wave components.

In all the cases considered herein, the variance was normalized in such a way that its initial value is always one. However, as is visible in all of the plots in figures 1a, 1b, 2a or 2b, the variance adjusts almost immediately to a somewhat larger value. This adjustment is a consequence of nonlinear interaction giving rise to new correlations among modes. During the time evolution, it was observed that several inhomogeneous terms $R_{i,j}$ were rapidly activated. Their contribution to the variance causes this fast, initial change in the variance.

The evolution of the system for depths of $h = 10$ m was also compared with the evolution over water of infinite depth. The latter yielded results that are indistinguishable from the plots in figures 1a, 1b, 2a and 2b.

5. Wave height statistics

We shall discuss three key statistics when describing ocean waves: the variance of the free surface elevation ρ, the root-mean-square wave height H_{rms} and the significant wave height H_s. The variance of the free surface ρ is the main outcome of the CSY equation, given in equation (25). At the wall, it is given by evaluating at $x = 0$. In the linear case, the variance is given by $\rho_0(0)$, see equation (14), and the values of H_{rms} and H_s are given in table 1. Note that the main difference between the linear variance and the nonlinear inhomogeneous one is that the latter is not stationary.

In order to use the time-dependent variance to establish wave height statistics we follow the approach developed by Regev et al. (2008). Their method consists in taking the Rayleigh distribution as a starting distribution for the wave heights, in accordance with the weakly Gaussian assumption. Then for any given time t

$$F(\hat{H},t) = P(H \leq \hat{H}) = 1 - \exp\left[-\frac{\hat{H}^2}{8\rho(0,t)}\right] = 1 - \exp\left[-\left(\frac{\hat{H}}{H_{rms}(t)}\right)^2\right]. \tag{40}$$

Note that in the last equality equation (33) was used for the time-dependent r.m.s. wave height.

Normalizing by H_{rms0}, which is obtained from equation (33) with $\rho_0(0)$ replacing $\rho(0,t)$, yields

$$F(\hat{H},t) = 1 - \exp\left[-\left(\frac{\hat{H}}{H_{rms0}}\right)^2 \frac{\rho_0}{\rho(0,t)}\right] = 1 - \exp\left[-\left(\frac{\hat{H}}{H_{rms0}}\right)^2 \frac{1}{\tilde{\rho}(0,t)}\right]. \tag{41}$$

Thus, at any give time t, the wave height probabilities can be obtained from the values of the normalized variance.

Table 3
Probability of freak wave occurrence computed for cases A–D (corresponding to different combinations of average wave slope ε and peak-sharpening parameter γ) and water depths from 1 m to 10 m, as well as the Rayleigh distribution. $P(\hat{H} > H_{s0})$ denotes the exceedance probability for the significant wave height, $P(\hat{H} > 2H_{s0})$ that for twice the significant wave height, and $P(\hat{H} > 3H_{s0})$ that for three times the significant wave height. For each case the ratios between the computed probabilities and those obtained from the Rayleigh distribution are shown in the columns labeled P/R.

Case	depth	$P(\hat{H} > H_{s0})$	P/R	$P(\hat{H} > 2H_{s0})$	P/R	$P(\hat{H} > 3H_{s0})$	P/R
A($\varepsilon = 0.1, \gamma = 3$)	1	0.14	1.08	3.73×10^{-4}	1.11	0.19×10^{-7}	1.27
	1.8	0.14	1.08	4.05×10^{-4}	1.21	0.23×10^{-7}	1.53
	3.6	0.14	1.08	4.16×10^{-4}	1.24	0.24×10^{-7}	1.60
	10	0.14	1.08	4.18×10^{-4}	1.24	0.25×10^{-7}	1.67
B($\varepsilon = 0.15, \gamma = 3$)	1	0.14	1.08	4.29×10^{-4}	1.28	0.26×10^{-7}	1.73
	1.8	0.15	1.15	5.25×10^{-4}	1.56	0.41×10^{-7}	2.73
	3.6	0.15	1.15	6.55×10^{-4}	1.95	1.31×10^{-7}	8.73
	10	0.15	1.15	10.3×10^{-4}	3.07	8.66×10^{-7}	59.1
C($\varepsilon = 0.1, \gamma = 10$)	1	0.14	1.08	3.74×10^{-4}	1.11	0.19×10^{-7}	1.27
	1.8	0.14	1.08	4.15×10^{-4}	1.24	0.24×10^{-7}	1.60
	3.6	0.14	1.08	4.95×10^{-4}	1.47	0.71×10^{-7}	4.73
	10	0.14	1.08	10.9×10^{-4}	3.24	19.69×10^{-7}	131.3
D($\varepsilon = 0.15, \gamma = 10$)	1	0.14	1.08	4.45×10^{-4}	1.32	0.3×10^{-7}	2
	1.8	0.15	1.15	6.12×10^{-4}	1.82	0.6×10^{-7}	4
	3.6	0.16	1.23	60.7×10^{-4}	18.07	1.2×10^{-4}	8000
	10	0.16	1.23	60.4×10^{-4}	17.98	1.0×10^{-4}	6666
Rayleigh	any	0.13		3.36×10^{-4}		0.15×10^{-7}	

In order to obtain wave height probabilities throughout the entire simulated time domain $[0, t_f]$ one time averages $F(\hat{H}, t)$ obtaining

$$F(\hat{H}) = \frac{1}{t_f}\int_0^{t_f} F(\hat{H}, \tau) d\tau. \tag{42}$$

In Regev et al. (2008) this last step is formally different, as the integration over time is replaced by an integral with respect to the probability density function of ρ. However, as noted by Andrade and Stiassnie (2020b), both approaches are equivalent.

The probability that the wave height exceeds a certain value is

$$P(H \geq \hat{H}) = 1 - F(\hat{H}). \tag{43}$$

This exceedance probability of the wave heights, obtained from the evolution of the normalized variance $\tilde{\rho}$, through equations (42) and (43), is influenced by depth. In the shallower cases, $h = 1$ m and $h = 1.8$ m, it is (essentially) Rayleigh distributed, regardless of ε and γ, i.e. for both narrow and broad banded spectra. This arises because the variance is nearly constant due to a lack of significant nonlinear interactions in such cases. Since the peak wave is $k_p = 1$ m^{-1}, the influence of depth rapidly diminishes as one considers deeper cases, so any deviation from the Rayleigh distribution is largely due to the spectral shape.

In Figure 3 we plot the exceedance probabilities for cases B, C and D and depths of $h = 3.6$ m and $h = 10$ m. Exact values of the probabilities are given in table 3, where we present the probability of freak-wave occurrence, i.e. waves whose wave height is larger than twice the significant wave height H_{s0}.

Note that Ribal et al. (2013), in an analysis based on the deep water Alber equation, find

$$P(\hat{H} > 2H_{s0}) = 10^{-(1.8+1.5\Pi)}, \tag{44}$$

whereas Andrade and Stiassnie (2020a,b), based on the deep water CSY equation, yield the somewhat higher values

$$P(\hat{H} > 2H_{s0}) = 10^{-(1.5+1.2\Pi)}. \tag{45}$$

For spectrum D (44) and (45) give $P(\hat{H} > 2H_{s0}) = 15 \times 10^{-4}$ and $P(\hat{H} > 2H_{s0}) = 40 \times 10^{-4}$, respectively. The latter compares quite well with the results for case D with depths $k_p h = 3.6, 10$.

Although we can compute the probability of extreme waves with wave heights higher than three times the significant wave height, and this is reported in table 3, such values must be treated cautiously in practice. Okamura (1987), Mercer and Roberts (1992) and others have given upper bounds on the steepness of standing waves, which were found to be $\varepsilon \approx 0.61$. Considering a typical wave around the spectral peak at $k_p = 1$ with wave height H, its steepness can be estimated as $k_p H/2$. Above this threshold, waves must be expected to break. In figure 3 the black vertical lines indicates the normalized wave heights that correspond to the breaking steepness. Thus, while it is formally possible to compute statistics for higher waves, these should be understood in the context of our model equations, which account for nonlinear wave-wave interaction only, but not for dissipation by wave breaking, wind input, or other potentially physically significant factors.

The statistics of a broad spectrum with moderate steepness, i.e. case A ($\gamma = 3$,$\varepsilon = 0.1$), were all governed by the Rayleigh distribution since, as seen from Figure 1a, there was no significant nonlinear interaction taking place at any depth. However, by increasing the steepness to $\varepsilon = 0.15$ (case B with $h = 3.6$ m and $h = 10$ m), the upper panels of figure 3 reveal an increase in exceedance probabilities. Such an increase is more pronounced in the deepest case. Likewise, as seen from table 3, there is about a three-fold increase in the probability of freak wave occurrence.

Surprisingly, the statistics obtained from a narrow spectrum ($\gamma = 10$) and steepness of $\varepsilon = 0.10$ were remarkably close to those of a broad spectrum ($\gamma = 3$) with $\varepsilon = 0.15$ at depths of $h = 3.6$ m and $h = 10$ m. Indeed, from the evolution of the spectral shape in figures 1b and 2a, one can see some minor energy exchange happening between the peak wave and its side bands, and almost no energy exchange away from it. Their variances reach comparable values and, in particular for $h = 3.6$ m, they have similar shapes. All these similarities are reflected in the statistics as well. Increasing the steepness of the narrow banded case (case D) greatly amplifies the exceedance probabilities of the wave heights, and in particular the probability of freak wave occurrence, which is increased by a factor of 18 for deeper depths, see table 3.

6. Discussion and conclusions

We have explored the effect of nonlinear four-wave interaction on stochastic wave fields reflected from a wall by means of the CSY equation. This equation can be solved to directly yield the time-evolution of the energy (variance) of a stochastic, weakly nonlinear wave field. In contrast to previous work, we extend this CSY equation to account for finite depth effects by a modification of the interaction kernels. As only wave fields in constant, finite depth are considered, the mathematically convenient JONSWAP spectrum is used to provide initial conditions for the incident waves.

What is the significance of these results? For waves impacting walls in moderate to large depths, the effects of nonlinear four-wave interactions on the energy of the wave field are significant, and are seen to increase with wave steepness, as has been shown in experimental work on wave-structure interaction by Sheikh and Swan (2005), Molin et al. (2005) and others. Considering the statistics of extreme waves at the wall, these are significantly altered, with a markedly increased probability of observing extreme waves above twice the significant wave-height.

We observe from the CSY that, although only the phases of incident and reflected waves are initially correlated (by virtue of the chosen initial conditions), this correlation quickly spreads among the modes. This serves to emphasize the important role of inhomogeneity in such interactions: for purely homogeneous evolution equations no evolution of the wave field is possible at this order of nonlinearity. The initial correlations begin a process wherein further correlations among the wave modes are activated, which in turn gives rise to spatio-temporal fluctuations of the variance (i.e. energy) throughout the wave field. One main conclusion of this work is that these fluctuations are associated with an increased probability of freak waves.

As the critical depth threshold of $k_p h \approx 1.363$ is approached from above, four-wave interaction effects grow weaker, as first reported by Benjamin (1967). This can be seen as a constraint between the peak wavelength and depth. Indeed, our results suggest a markedly increased probability of freak waves for $k_p h > 3.6$, meaning that the peak wavelength must be shorter than roughly twice the depth. For the shallowest cases reported herein, the vast majority of wave modes in the spectra studied undergo no meaningful interaction. Instead, in shallow waters near-resonant three wave interactions become increasingly important, as do other bottom effects (see Stuhlmeier et al. (2019)). To further explore such cases, an inclusion of nearly resonant three-wave interactions, using e.g. the full, and substantially more cumbersome equation (14.2.14) of Mei et al. (2018) as point of departure may be of interest.

A second condition which governs an increased probability of freak wave occurrence for waves reflected in water of constant depth is that of a narrow attacking spectrum. Indeed, using the dimensionless parameter $\Pi = \varepsilon/\alpha\gamma$, introduced by Ribal et al. (2013) as measure of narrowness, we found that, for Π less than or approximately equal to unity the wave field is prone to produce freak-waves. This can be realised for large values of γ or steep wave fields, i.e. large values of ε. Otherwise the statistics of the random wave field are effectively linear and the likely hood of observing freak-waves is predicted by the Rayleigh distribution.

The depth of $h = 1.8$ m is comparable to that used in the experiments of Voermans et al. (2020). The choice of JONSWAP parameters and steepness of the attacking waves in our cases A and B, i.e. $\gamma = 3$ and $\varepsilon = 0.1$, $\varepsilon = 0.15$ respectively, were made to compare with their experimental data. The results from our model show that the resulting standing wave field shares similar statistical properties with those obtained from a field of linear standing waves; the amplitude of the waves at the wall is twice the amplitude of the attacking waves, and their steepness is doubled accordingly. This could provide a theoretical explanation for some of their conclusions.

One critical issue that cannot be addressed within the present formalism, stemming as it does from the deterministic Zakharov equation, is wave breaking. As noted above, the exceedance probabilities for extreme waves can be readily computed for arbitrary values of the wave height, but non-breaking standing waves should not be expected above $\varepsilon \approx 0.61$. However, the Zakharov equation which forms the basis for the stochastic CSY model does not include the effects of dissipation. It may be possible to remedy this situation, along the lines of work by Annenkov and Shrira (2013), by introducing dissipation and rederiving a form of the stochastic CSY equation. A further possibility would be to explore alternatives to the Rayleigh distribution, such as the composite Weibull distribution of Battjes and Groenendijk (2000), which offers an adjustment to the Rayleigh distribution in water of finite depth which takes into account wave breaking. Both of these alternatives would offer fruitful avenues for future work.

Recent years have also seen a great deal of interest in the incidence of freak waves on variable depth, see e.g. Gramstad et al. (2013); Kashima and Mori (2019). As the underlying, deterministic Zakharov equation has been derived only for constant depth, the present approach is not directly applicable. Indeed, while Iusim and Stiassnie (1985) extended the cubic self-interaction Zakharov kernel $T(k, k, k, k)$ to include the effects of slow depth variation, a general form for arbitrary quartets is still unknown. Recently work has been undertaken to extend the narrow-bandwidth Alber equation to a sloping bed by Kluczek et al. (2021), although this unidirectional model cannot include the effects of reflection.

Although we have concentrated herein on the reflection of waves from a wall, the methods and analysis developed can be applied to other types of obstacles. For instance, following Ursell (1947), one could consider submerged barriers. In this case the CSY equation used herein remains unchanged, while the initial correlations would be modified by the reflection coefficients. Likewise, it would be natural to extend the present work to directional spectra and thus waves incident from multiple angles, which would however require a considerable increase in computational resource. These and other related problems provide material for significant future work.

A. Appendix

The symmetric Zakharov kernels in finite depth exhibit singularities, and therefore require careful treatment. These kernels may be split into two parts (here we follow Stiassnie and Gramstad (2009)):

$$T_{j,j,j,j} = T^R_{j,j,j,j} + T^S_{j,j,j,j}. \tag{46}$$

$$T_{j,m,j,m} = T^R_{j,m,j,m} + T^S_{j,m,j,m}. \tag{47}$$

The superscript R denotes the so-called regular part and superscript S the singular part of these kernels.

The kernels $T_{p,p,p,p}$ and $T_{p,-p,p,-p}$ are particularly important, as they govern the modulational instability of a single wave-train and the interaction between an incident wave and its reflection, respectively. For a wave $k_p = 1$ m^{-1} and depths ranging from 0.5 m to 3 m, these two symmetric kernels are plotted in figure 4, normalized by their infinite-depth values $T_{p,p,p,p} = -T_{p,-p,p,-p} = k_p^3/4\pi^2$. Note that $T_{p,p,p,p}$ changes sign at $k_p h = 1.363$ and $T_{p,-p,p,-p}$ does so at $k_p h = 1.04$. As the depth tends to zero, both kernels tend to infinity and when the depth tends to infinity, the singular part vanishes and one recovers the usual values of the infinite depth Zakharov kernel.

The analytical expressions of these kernels used throughout the paper are given in the following. Recall that we are in one spatial dimension, and therefore write all wave vectors $\mathbf{k}_j = (k_j, 0)$. We employ the finite depth dispersion relation $\omega_j^2 = gk_j \tanh(k_j h)$ throughout. The regular parts of the kernels are

$$T^R_{j,j,j,j} = \frac{k_j^2}{32\pi^2 g\omega_j^6}\left(9\omega_j^8 - 10g^2k_j^2\omega_j^4 + 9g^4k_j^4\right). \tag{48}$$

$$\begin{aligned}
T^R_{j,m,j,m} =& \frac{g}{32\pi^2\omega_j\omega_m}\Bigg\{ -2\frac{\omega_j^2\omega_m^2}{g^2}\left(k_j^2 + k_m^2\right) \\
&+ \frac{1}{\omega_{j-m}^2 - (\omega_j - \omega_m)^2}\Bigg\{\left[\omega_m(k_j^2 - k_jk_m) - \omega_j(k_m^2 - k_jk_m)\right] \\
&\times\left[-\omega_m(k_j^2 - 3k_jk_m) + \omega_j(k_m^2 - 3k_jk_m) + 2\frac{\omega_j^2\omega_m^2}{g^2}(\omega_j - \omega_m)\right] \\
&- \omega_{j-m}^2\Bigg[(k_jk_m)^2 + 2\frac{\omega_j\omega_m^3}{g^2}(k_j^2 - 2k_jk_m) - 2\frac{\omega_j^2\omega_m^2}{g^2}(k_j^2 + k_m^2 - 3k_jk_m) \\
&+ 2\frac{\omega_j^3\omega_m}{g^2}(k_m^2 - 2k_jk_m) + \frac{\omega_j^2\omega_m^2}{g^4}(\omega_j^2 - \omega_j\omega_m + \omega_m^2)^2\Bigg]\Bigg\} \\
&- \frac{1}{\omega_{j+m}^2 - (\omega_j + \omega_m)^2}\Bigg\{\left[\omega_m(k_j^2 + k_jk_m) + \omega_j(k_m^2 + k_jk_m)\right] \\
&\times\left[\omega_m(k_j^2 + 3k_jk_m) + \omega_j(k_m^2 + 3k_jk_m) + 2\frac{\omega_j^2\omega_m^2}{g^2}(\omega_j + \omega_m)\right] \\
&\omega_{j+m}^2\Bigg[(k_jk_m)^2 - 2\frac{\omega_j\omega_m^3}{g^2}(k_j^2 + 2k_jk_m) - 2\frac{\omega_j^2\omega_m^2}{g^2}(k_j^2 + k_m^2 + 3k_jk_m) \\
&- 2\frac{\omega_j^3\omega_m}{g^2}(k_m^2 + 2k_mk_j) + \frac{\omega_j^2\omega_m^2}{g^4}(\omega_j^2 + \omega_j\omega_m + \omega_m^2)^2\Bigg\}\Bigg\}.
\end{aligned} \tag{49}$$

These equations correspond to equations (3.8b) and (3.9b) of Stiassnie and Gramstad (2009).

The singular parts of the kernels are:

$$T^S_{j,j,j,j} = -\frac{g}{16\pi^2}\frac{4k_j^2\left[1+\frac{C_{g_j}}{k_j\omega_j}\left(k_j^2-\frac{\omega_j^4}{g^2}\right)\right]+\frac{gh}{\omega_j^2}\left(k_j^2-\frac{\omega_j^4}{g^2}\right)^2}{gh-{C_{g_j}}^2}. \tag{50}$$

In this equation C_{g_j} denotes the group velocity of the wave k_j. This equation corresponds to equation (4.10) of Stiassnie and Gramstad (2009), except for a misprint corrected by Xu et al. (2012).

The singular part of the kernel is

$$\begin{aligned} T^S_{j,m,j,m} =& -\frac{g}{32\pi^2(gh-{C_{g_m}}^2)}\left\{\left(k_j^2-\frac{\omega_j^4}{g^2}\right)\left(k_m^2-\frac{\omega_m^4}{g^2}\right)\frac{gh}{2\omega_j\omega_m}\right. \\ &\left.+k_jk_m\left[2+\frac{C_{g_m}}{k_m\omega_m}\left(k_m^2-\frac{\omega_m^4}{g^2}\right)\right]+\frac{C_{g_m}k_m}{\omega_j}\left(k_j^2-\frac{\omega_j^4}{g^2}\right)\right\} \\ &-\frac{g}{32\pi^2(gh-{C_{g_j}}^2)}\left\{\left(k_j^2-\frac{\omega_j^4}{g^2}\right)\left(k_m^2-\frac{\omega_m^4}{g^2}\right)\frac{gh}{2\omega_j\omega_m}\right. \\ &\left.+k_jk_m\left[2+\frac{C_{g_j}}{k_j\omega_j}\left(k_j^2-\frac{\omega_j^4}{g^2}\right)\right]+\frac{C_{g_j}k_j}{\omega_m}\left(k_m^2-\frac{\omega_m^4}{g^2}\right)\right\}. \end{aligned} \tag{51}$$

This equation corresponds to equation (5.1) of Stiassnie and Gramstad (2009) in one dimension. We point out that the original equation, derived in two dimensions, is not uniquely defined, however in one spatial dimension such indefiniteness vanishes.

CRediT authorship contribution statement

David Andrade: Writing - Original Draft, Software, Investigation. **Raphael Stuhlmeier:** Writing - Review and Editing, Validation, Funding acquisition. **Michael Stiassnie:** Conceptualization, Supervision, Funding acquisition.

References

Alber, I.E., 1978. The effects of randomness on the stability of two-dimensional surface wavetrains. Proceedings of the Royal Society A: Mathematical, Physical and Engineering Sciences 363, 525–546. doi:10.1098/rspa.1978.0181.

Andrade, D., Stiassnie, M., 2020a. Bound-waves due to sea and swell trigger the generation of freak-waves. Journal of Ocean Engineering and Marine Energy 6, 399–414. doi:10.1007/s40722-020-00179-3.

Andrade, D., Stiassnie, M., 2020b. New solutions of the C.S.Y. equation reveal increases in freak wave occurrence. Wave Motion , 102581doi:10.1016/j.wavemoti.2020.102581.

Annenkov, S.Y., Shrira, V.I., 2013. Large-time evolution of statistical moments of wind–wave fields. J. Fluid Mech. 726, 517–546. doi:10.1017/jfm.2013.243.

Athanassoulis, A., Gramstad, O., 2021. Modelling of ocean waves with the Alber equation: application to non-parametric spectra and generalization to crossing seas URL: http://arxiv.org/abs/2105.00102, arXiv:2105.00102.

Battjes, J.A., Groenendijk, H.W., 2000. Wave height distributions on shallow foreshores. Coastal engineering 40, 161–182.

Benjamin, T.B., 1967. Instability of periodic wavetrains in nonlinear dispersive systems. Proc. R. Soc. London. Ser. A. Math. Phys. Sci. 299, 59–76. doi:10.1098/rspa.1967.0123.

Bryant, P.J., Stiassnie, M., 1994. Different forms for Nonlinear Standing Waves in Deep Water. J. Fluid Mech. 272, 135–156. doi:10.1017/S0022112094004416.

Bullock, G.N., Obhrai, C., Peregrine, D.H., Bredmose, H., 2007. Violent breaking wave impacts. Part 1: Results from large-scale regular wave tests on vertical and sloping walls. Coast. Eng. 54, 602–617. doi:10.1016/j.coastaleng.2006.12.002.

Christou, M., Hague, C.H., Swan, C., 2009. The reflection of nonlinear irregular surface water waves. Eng. Anal. Bound. Elem. 33, 644–653. doi:10.1016/j.enganabound.2008.10.005.

Crawford, D.R., Saffman, P.G., Yuen, H.C., 1980. Evolution of a random inhomogeneous field of nonlinear deep-water gravity waves. Wave Motion 2, 1–16. doi:10.1016/0165-2125(80)90029-3.

Dawson, D., Shaw, J., Roland Gehrels, W., 2016. Sea-level rise impacts on transport infrastructure: The notorious case of the coastal railway line at Dawlish, England. J. Transp. Geogr. 51, 97–109. doi:10.1016/j.jtrangeo.2015.11.009.

Gramstad, O., 2017. Modulational Instability in JONSWAP Sea States Using the Alber Equation, in: ASME 2017 36th Int. Conf. Ocean. Offshore Arct. Eng., ASME, Trondheim, Norway. p. V07BT06A051. URL: http://proceedings.asmedigitalcollection.asme.org/proceeding.aspx?doi=10.1115/OMAE2017-61671, doi:10.1115/OMAE2017-61671.

Gramstad, O., Stiassnie, M., 2013. Phase-averaged equation for water waves. J. Fluid Mech. 718, 280–303. doi:10.1017/jfm.2012.609.

Gramstad, O., Zeng, H., Trulsen, K., Pedersen, G.K., 2013. Freak waves in weakly nonlinear unidirectional wave trains over a sloping bottom in shallow water. Phys. Fluids 25, 122103. URL: http://aip.scitation.org/doi/10.1063/1.4847035, doi:10.1063/1.4847035.

Hattori, M., Arami, A., Yui, T., 1994. Wave impact pressure on vertical walls under breaking waves of various types. Coast. Eng. 22, 79–114. doi:10.1016/0378-3839(94)90049-3.

Holthuijsen, L.H., 2010. Waves in oceanic and coastal water. Cambridge university press.

Iusim, R., Stiassnie, M., 1985. Shoaling of nonlinear wave groups on water of slowly varying depth. Zeitschrift für Angew. Math. und Phys. 36, 680–698.

Janssen, P.A.E.M., Onorato, M., 2007. The Intermediate Water Depth Limit of the Zakharov Equation and Consequences for Wave Prediction. J. Phys. Oceanogr. 37, 2389–2400. doi:10.1175/jpo3128.1.

Kashima, H., Mori, N., 2019. Aftereffect of high-order nonlinearity on extreme wave occurrence from deep to intermediate water. Coast. Eng. 153, 103559. URL: https://doi.org/10.1016/j.coastaleng.2019.103559, doi:10.1016/j.coastaleng.2019.103559.

Kluczek, M., Andrade, D., Stiassnie, M., 2021. On the Alber equation for shoaling water waves. preprint .

Krasitskii, V.P., 1994. On reduced equations in the hamiltonian theory of weakly nonlinear surface waves. Journal of Fluid Mechanics 272, 1–20. doi:10.1017/S0022112094004350.

Liu, S., Gatin, I., Obhrai, C., Ong, M.C., Jasak, H., 2019. CFD simulations of violent breaking wave impacts on a vertical wall using a two-phase compressible solver. Coast. Eng. 154, 103564. doi:10.1016/j.coastaleng.2019.103564.

Mei, C.C., Stiassnie, M.A., Yue, D.K.P., 2018. Theory and Applications of Ocean Surface Waves: Part 2: Nonlinear Aspects. 3 ed., World Scientific.

Mercer, G.N., Roberts, A.J., 1992. Standing waves in deep water: Their stability and extreme form. Phys. Fluids A 4, 259–269. doi:10.1063/1.858354.

Molin, B., Remy, F., Kimmoun, O., Jamois, E., 2005. The role of tertiary wave interactions in wave-body problems. J. Fluid Mech. 528, 323–354. doi:10.1017/S002211200500340X.

Okamura, M., 1987. Maximum wave steepness and instabilities of finite-amplitude standing gravity waves. Fluid dynamics research 1, 201.

Regev, A., Agnon, Y., Stiassnie, M., Gramstad, O., 2008. Sea swell interaction as a mechanism for the generation of freak waves. Physics of Fluids 20, 112102. doi:10.1063/1.3012542.

Ribal, A., Babanin, A.V., Young, I., Toffoli, A., Stiassnie, M., 2013. Recurrent solutions of the Alber equation initialized by joint north sea wave project spectra. Journal of Fluid Mechanics 719, 314–344. doi:10.1017/jfm.2013.7.

Sheikh, R., Swan, C., 2005. The interaction between steep waves and a vertical, surface-piercing column. J. Offshore Mech. Arct. Eng. 127, 31–38. doi:10.1115/1.1854701.

Stiassnie, M., Gramstad, O., 2009. On zakharov's kernel and the interaction of non-collinear wavetrains in finite water depth. Journal of fluid mechanics 639, 433. doi:10.1017/S002211200999173X.

Stuhlmeier, R., Stiassnie, M., 2019. Evolution of statistically inhomogeneous degenerate water wave quartets. Philosophical Transactions of the Royal Society A: Mathematical, Physical and Engineering Sciences 376, 20170101. doi:10.1098/rsta.2017.0101.

Stuhlmeier, R., Vrecica, T., Toledo, Y., 2019. Nonlinear wave interaction in coastal and open seas – deterministic and stochastic theory, in: Henry, D., Kalimeris, K., Parau, E., Vanden-Broeck, J.M., Wahlen, E. (Eds.), Nonlinear Water Waves. Springer, pp. 151–181. arXiv:1909.04348.

Ursell, F., 1947. The effect of a fixed vertical barrier on surface waves in deep water. Mathematical Proceedings of the Cambridge Philosophical Society 43, 374–382. doi:10.1017/S0305004100023604.

Voermans, J.J., Laface, V., Babanin, A.V., Romolo, A., Arena, F., 2020. Standing wave field observations at a vertical wall. Coastal Engineering 160, 103749. doi:10.1016/j.coastaleng.2020.103749.

Xu, D., Lin, Z., Liao, S., Stiassnie, M., 2012. On the steady-state fully resonant progressive waves in water of finite depth. Journal of Fluid Mechanics 710, 379–418. doi:10.1017/jfm.2012.370.

Zakharov, V.E., 1968. Stability of periodic waves of finite amplitude on the surface of a deep fluid. Journal of Applied Mechanics and Technical Physics 9, 190–194. doi:10.1007/bf00913182.

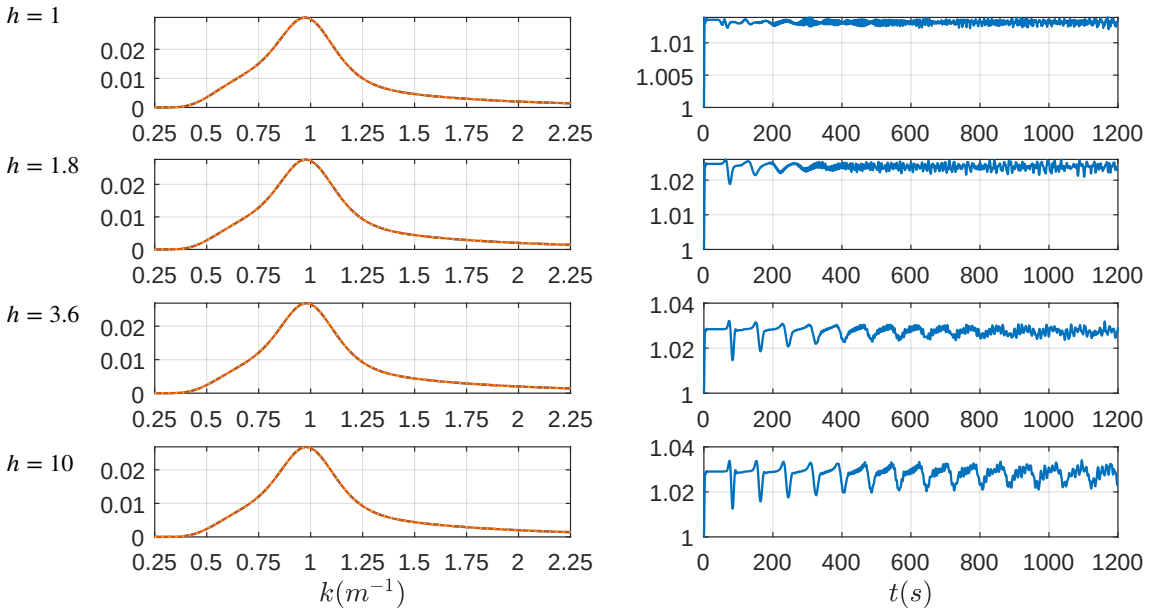

(a) Cases A ($\varepsilon = 0.1, \gamma = 3$). Left plots: Results of the time evolution of R_{ii}. Right plots: Normalized variance $\tilde{\rho}(0,t)$.

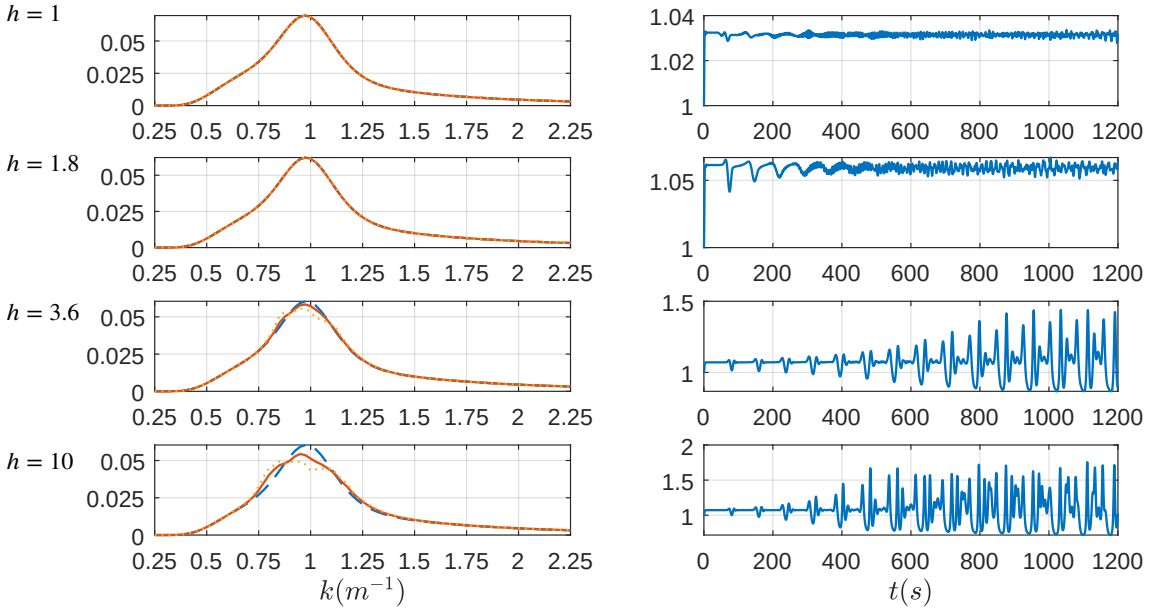

(b) Cases B ($\varepsilon = 0.15, \gamma = 3$). Left plots: Results of the time evolution of R_{jj}. Right plots: Normalized variance $\tilde{\rho}(0,t)$.

Figure 1: Numerical simulations for broad banded ($\gamma = 3$) JONSWAP spectra at various water depths. Left panels: results of the spectral time evolution, for the incoming waves. The blue dashed line is the initial spectrum. The red solid line is the time-averaged spectrum. The yellow dotted line is the spectrum at $t_f = 1200s$. Right panels: time series of the normalized variance of the free surface at $x = 0$.

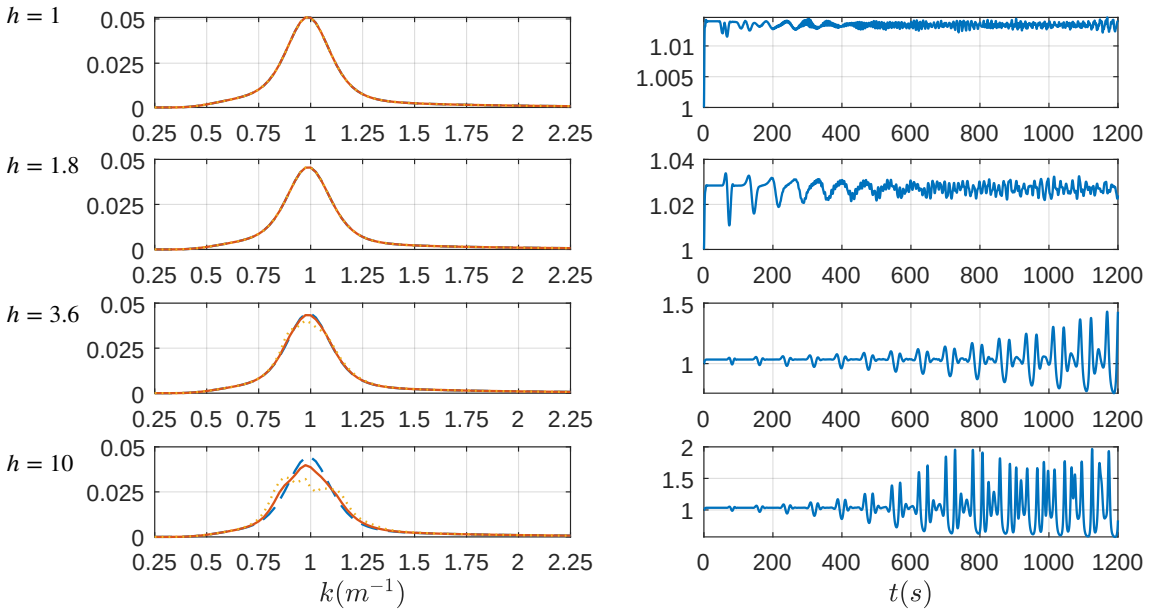

(a) Cases C ($\epsilon = 0.1, \gamma = 10$). Left plots: Results of the time evolution of R_{ii}. Right plots: Normalized variance $\tilde{\rho}(0,t)$.

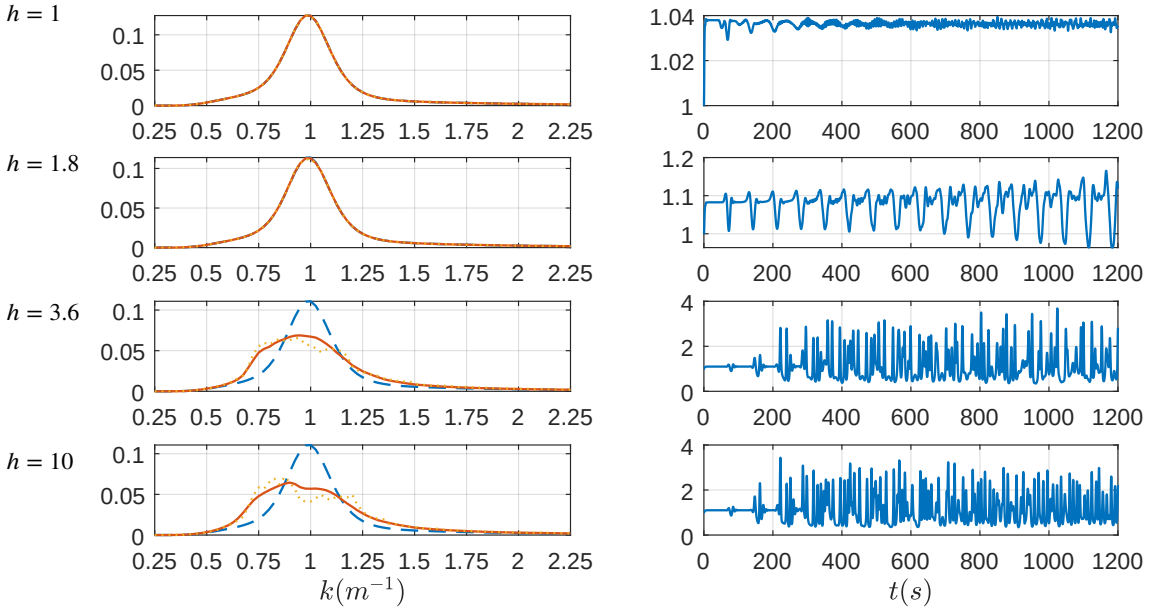

(b) Cases D ($\epsilon = 0.15, \gamma = 10$). Left plots: Results of the time evolution of R_{jj}. Right plots: Normalized variance $\tilde{\rho}(0,t)$.

Figure 2: Numerical simulations for narrow banded ($\gamma = 10$) JONSWAP spectra at various water depths. Left panels: results of the spectral time evolution, for the incoming waves. The blue dashed line is the initial spectrum. The red solid line is the time-averaged spectrum. The yellow dotted line is the spectrum at $t_f = 1200s$. Right panels: time series of the normalized variance of the free surface at $x = 0$.

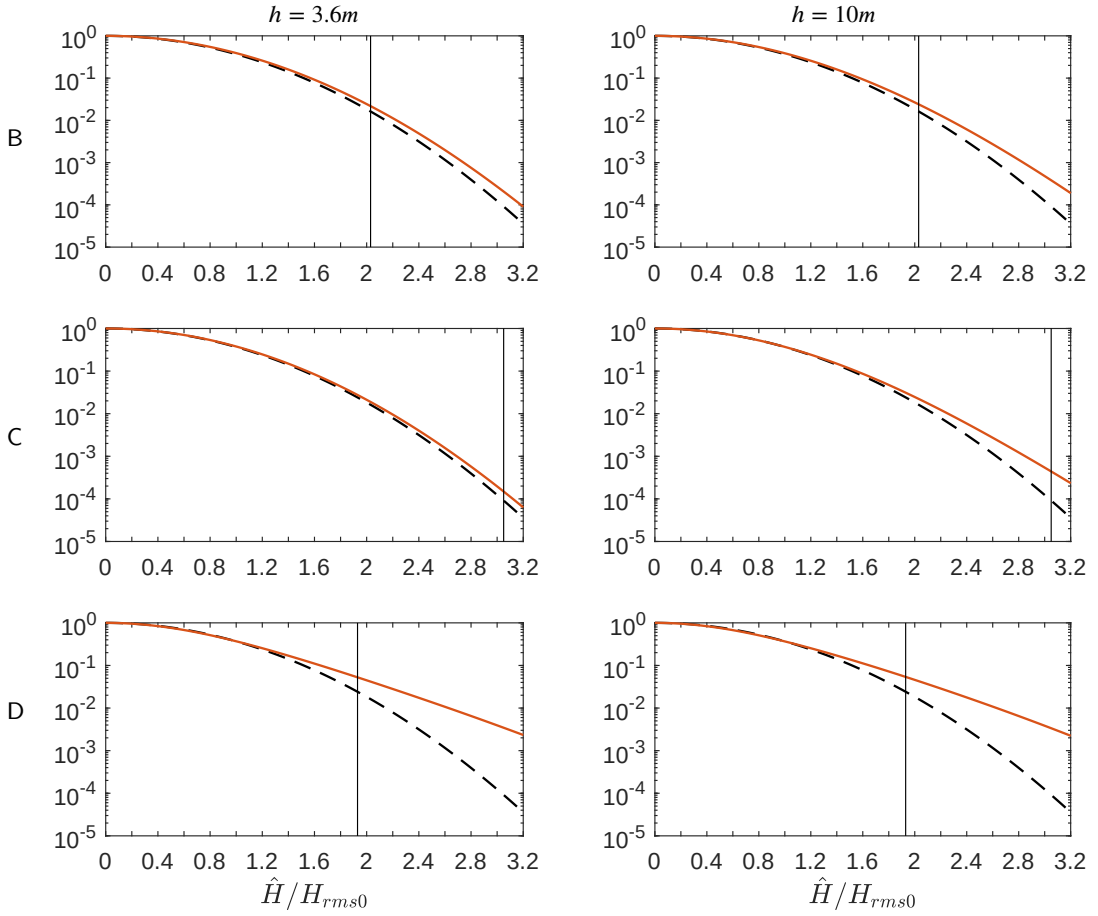

Figure 3: Exceedance probabilities for the wave height normalized by H_{rms0} in Cases B, C, and D for depths of $h = 3.6$ m and $h = 10$ m. Red solid line: $P(H \geq \hat{H})$ computed from the CSY equation. Black dashed line: probabilities taken from the Rayleigh distribution. $\hat{H} = H_{s0}$ at 1.42 and $\hat{H} = 2H_{s0}$ at 2.82. Values to the right of the black vertical line have a steepness in excess of the approximate breaking threshold of 0.61.

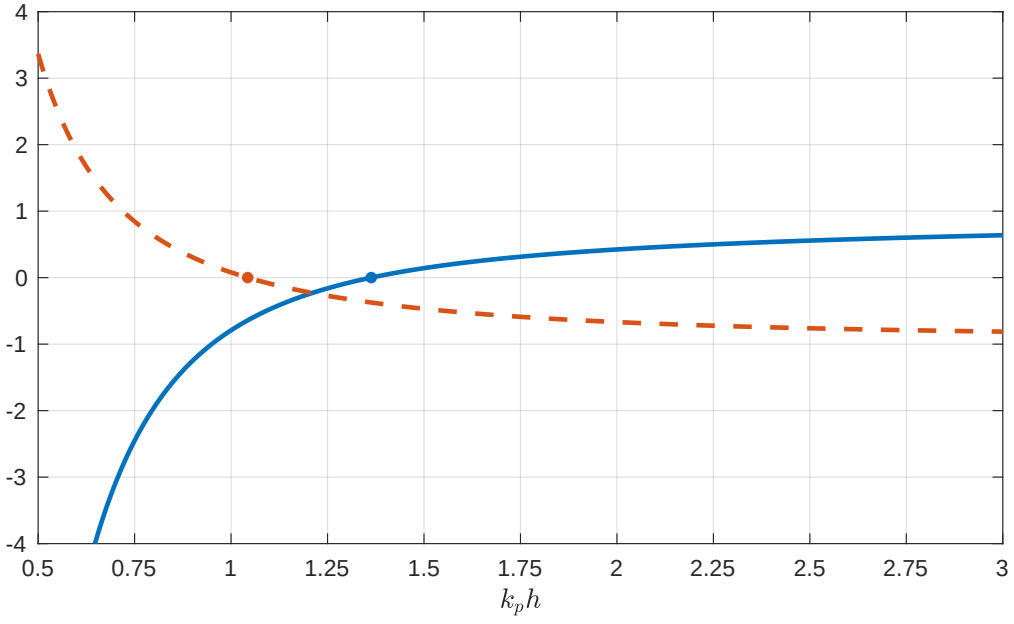

Figure 4: Plot of the kernels $4\pi^2 T_{p,p,p,p}$ (blue solid line) and $4\pi^2 T_{p,-p,p,-p}$ (red broken line) as a function of dimensionless depth. The subscript p stands for the peak wave $k_p = 1$ m^{-1}. The kernel $T_{p,p,p,p}$ vanishes at $k_p h = 1.363$ and $T_{p,-p,p,-p}$ vanishes at $k_p h = 1.04$. For $k_p h$ tending to infinity the solid and broken lines approach the values of 1 and -1 respectively.